Organic Geochemistry 194 (2024) 104780

Contents lists available at ScienceDirect

Organic Geochemistry

journal homepage: www.elsevier.com/locate/orggeochem

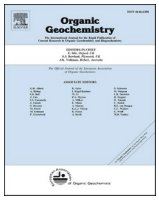

Impact of water depth on the distributions and proxies of isoprenoidal hydroxylated GDGTs in the Mediterranean Sea and the Red Sea

Devika Varma [a,*], Marcel T.J. van der Meer [a], Gert-Jan Reichart [b,c], Stefan Schouten [a,c]

[a] NIOZ Royal Netherlands Institute for Sea Research, Department of Marine Microbiology and Biogeochemistry, P.O. Box 59, 1790 AB Den Burg, Texel, The Netherlands
[b] NIOZ Royal Netherlands Institute for Sea Research, Department of Ocean Systems, P.O. Box 59, 1790 AB Den Burg, Texel, The Netherlands
[c] Utrecht University, Department of Earth Sciences, Faculty of Geosciences, Princetonlaan 8a, 3584 CD Utrecht, The Netherlands

ARTICLE INFO

Associate Editor — J. Volkman

Keywords:
Hydroxylated GDGT
TEX_{86}
RI-OH
%OH
Mediterranean Sea
Red Sea

ABSTRACT

Hydroxylated Isoprenoidal Glycerol Dialkyl Glycerol Tetraethers (OH-isoGDGTs) have recently been utilized as paleothermometers in the marine environment. However, their ability to reconstruct temperature in the Mediterranean and Red Sea has not been adequately investigated. Previous research has shown that archaeal communities inhabiting different water depths in these basins exert a substantial influence on the regular isoGDGT distributions and associated proxies such as the TEX_{86}. However, the impact of these archaea on OH-isoGDGTs and their corresponding proxies remains unclear. In this study, we examined the distribution of OH-isoGDGTs and their associated proxies (%OH, RI-OH, RI-OH′ and TEX_{86}^{OH}) in surface sediments of the Mediterranean and the Red Sea. We observe strong correlations between the fractional abundances of OH-isoGDGTs, relative to all isoGDGTs and OH-isoGDGTs, and water depth which suggests that deep-water archaeal communities have a lower OH-isoGDGT abundance compared to the shallow communities. As a result, %OH and TEX_{86}^{OH} are strongly correlated with water depth, particularly at depths <500 m in the Mediterranean Sea. Interestingly, RI-OH and RI-OH′ show no correlation with water depth in the Mediterranean Sea. Instead, they correlate more strongly with satellite-derived sea surface temperature compared to other isoGDGT-based proxies, indicating their potential as paleothermometers. Finally, unlike TEX_{86} and TEX_{86}^{OH}, the %OH, RI-OH and RI-OH′ do not exhibit distinct 'Red Sea cluster' and display comparable values to sediments from other tropical oceans. Further research on sedimentary OH-isoGDGT distributions with broader geographical coverage within these basins and enrichment cultures of deep-water archaea are needed to confirm these observations.

1. Introduction

Isoprenoidal glycerol dialkyl glycerol tetraethers (isoGDGTs) are lipids produced mainly by Thaumarchaeota (now known as *Nitrososphaeria* in the Global Taxonomy Database; Rinke et al., 2021) in the marine environment (Sinninghe Damsté et al., 2002; Schouten et al., 2013; Tierney, 2014; Zeng et al., 2019). They are commonly employed in paleoclimatology to reconstruct past environmental conditions, particularly using the paleothermometer known as TEX_{86} (TetraEther indeX of 86 carbons; Schouten et al., 2002). However, there are several limitations associated with the TEX_{86} proxy. For instance, seasonal and depth variations in the source signal can introduce biases in temperature estimates (e.g., Huguet et al., 2007; Jia et al., 2012), while input of isoGDGTs from land can severely impact the TEX_{86} (e.g., Weijers et al., 2011).

Studies involving suspended particulate matter and sediments have demonstrated that in addition to temperature, the isoGDGT distribution can also be influenced by contributions from different archaeal communities in the water column (Basse et al., 2014; Kim et al., 2015, 2016; Jia et al., 2017; Hurley et al., 2018). This is primarily indicated by increasing isoGDGT [2]/[3] ratios with increasing water depth (e.g., Taylor et al., 2013; Hernández-Sánchez et al., 2014; Kim et al., 2016; Hurley et al., 2018) which has been linked to different archaeal communities in shallow and deep waters, as indicated by molecular ecological studies (e.g., Villanueva et al., 2015; Besseling et al., 2019). This relationship between the isoGDGT [2]/[3] ratio and water depth has been found globally in the marine environment and has been utilized to unravel changes in sedimentary contributions of shallow and deep water communities over time (Taylor et al., 2013; Hurley et al., 2018; Rattanasriampaipong et al., 2022). Generally, however, TEX_{86} values

* Corresponding author.
E-mail address: devika.varma@nioz.nl (D. Varma).

https://doi.org/10.1016/j.orggeochem.2024.104780
Received 4 March 2024; Received in revised form 4 April 2024; Accepted 8 April 2024
Available online 9 April 2024

are not affected by this changing ratio because isoGDGT-2 and -3 are present in both the numerator and the denominator of the index, and thus TEX_{86} generally does not correlate with water depth. In contrast, large changes in TEX_{86} with water depth have been observed in the Mediterranean Sea (Kim et al., 2015; Besseling et al., 2019). In particular, the fractional abundance of isoGDGT-2 and the crenarchaeol isomer (cren') increase as water depth increases, while isoGDGT-3 decreases (Kim et al., 2015). The increase in the fractional abundance of cren' with water depth results in a higher TEX_{86}, which introduces a warm bias when reconstructing temperature from Mediterranean Sea sediments (e.g., Huguet et al., 2011; Nieto-Moreno et al., 2013; Polik et al., 2018). To date, it remains unclear why this depth trend occurs in this semi-enclosed basin, in contrast to the open marine environment.

The nearby Red Sea is another land-locked basin with high temperature and salinity and is associated with distinct vertically distributed endemic populations of archaea adapted to such environments (Eder et al., 2002; Qian et al., 2011). This is reflected in isoGDGT distributions in surface sediments from the Red Sea, which is characterized by high cren' abundance compared to temperature-equivalent tropical sediments (Trommer et al., 2009; Inglis et al., 2015). Consequently, they form a distinctly separate cluster in the global TEX_{86}-sea surface temperature (SST) relationship (Trommer et al., 2009; Kim et al., 2010). Interestingly, Kim et al. (2015) showed that the Red Sea data showed a similar pattern as the deep-water sediments (>1000 m depth) from the Mediterranean Sea, i.e., they collectively showed an excellent correlation ($R^2 = 0.94$) with sea surface temperature. The exact cause of this observation remains to be elucidated.

Hydroxylated isoGDGTs (OH-isoGDGTs) are compounds ubiquitously found in the marine environment and also thought to be mainly derived from Thaumarchaeota (Liu et al., 2012; Sinninghe Damsté et al., 2012; Elling et al., 2017). Like isoGDGTs, they have been employed in the development of various temperature proxies such as %OH (Huguet et al., 2013), RI-OH′ and RI-OH (Lü et al., 2015), and, more recently, TEX_{86}^{OH} (TetraEther indeX of 86 carbon atoms including OH-isoGDGT-0; Varma et al., 2024). OH-isoGDGTs are known to be more abundant at higher latitudes in the global ocean (Huguet et al., 2013), and they are suggested to serve as a low temperature adaptation for archaeal cells by increasing the fluidity of the cell membrane (Huguet et al., 2017). The ring indices of hydroxylated isoGDGTs, RI-OH′ and RI-OH have also shown promise in paleotemperature reconstructions, especially in the Mediterranean region (Davtian et al., 2019; Morcillo-Montalbá et al., 2021). The potential application of OH-isoGDGT-based temperature proxies in the Mediterranean region is intriguing, as previous attempts to utilize the TEX_{86} paleothermometer in this region have been hindered by the strong depth-related trends in isoGDGT distributions discussed above (Leider et al., 2010; Grauel et al., 2013; Kim et al., 2015). This raises the question of whether OH-isoGDGT-based proxies might be more effective as temperature proxies in the Mediterranean, and possibly the Red Sea, compared to isoGDGT-based proxies.

Here, we analyzed the distributions of OH-isoGDGTs in surface sediments from the Mediterranean Sea and the Red Sea to establish the impact of water depth, as well as temperature on these compounds, in comparison to regular isoGDGTs. The implications of these results for OH-isoGDGT-based temperature proxies in these environments, as well as their application, are discussed.

2. Materials and methods

2.1. Study areas and surface sediments

2.1.1. Mediterranean Sea

The semi-enclosed basin of the Western Mediterranean Sea is characterized by a dynamic interplay of surface water masses coming from the Atlantic Ocean via the Strait of Gibraltar, Levantine Intermediate Water originating from the Eastern Mediterranean Sea through the Strait of Sicily, and the Mediterranean deep water that is formed in the Gulf of Lions (MEDOC Group, 1970; Rohling et al., 2009). Nineteen surface sediments were obtained from the Balearic Sea near the Balearic Islands, where water depth varies markedly within a confined spatial extent, as described by Kim et al. (2015) (Fig. 1a). The sediments were retrieved within a small geographical area (~100 by 50 km) with large difference in water depth between the surface sediments ranging from 150 to 780 m. The 10-yr average satellite-derived SST data from NSIPP AVHRR (Advanced Very High Resolution Radiometer) was obtained after Kim et al. (2015) and utilized in this study. They range from 18.8 to 19.5 °C for this region. The sea surface salinity (SSS) in this region varies between 37.4 and 37.9 mg/g (from 0.25° grid database of World Ocean Atlas WOA18; Zweng et al., 2019). These sediments were analyzed previously for non-hydroxylated isoGDGTs (Kim et al., 2015), and were re-analyzed for OH-isoGDGTs in this study using an updated method (Hopmans et al., 2016). These data were combined with OH-isoGDGT and isoGDGT data from 57 surface sediments from the Gulf of Lions which were previously published (Varma et al., 2024). These surface sediments were retrieved from water depths as shallow as 8 m to as deep as 2370 m. Satellite-derived SST in this location ranged from 16.5 to 17.2 °C and salinity between 36.6 and 38.2 mg/g (Zweng et al., 2019). Unfortunately, other surface sediments from Kim et al. (2015) and suspended particulate matter samples from Kim et al. (2015) and Besseling et al. (2019) were not available for this study as they were either fully depleted or could not be retrieved from the NIOZ storage.

2.1.2. Red Sea

The Red Sea is a tropical oceanographic basin characterized by strong temperature and salinity gradients extending from the northern to the southern part of the narrow basin. It is connected to the Indian Ocean at the southern end through the narrow Strait of Bab el Mandeb. The annual mean SST and SSS ranges from ~25 to 29 °C and ~37 to 41.6, respectively, along this gradient (Trommer et al., 2009; Zweng et al., 2019). A total of 9 surface sediments from the northern Red Sea and 6 surface sediments from the southern Red Sea (Fig. 1b) were utilized in this study, which were previously examined for isoGDGTs and TEX_{86} at NIOZ (Trommer et al., 2009) and re-analyzed here for OH-isoGDGTs. As mentioned in Trommer et al. (2009), the 0–5 cm depth interval of these sediments were not available as they were stored in Rose Bengal stain in alcohol. Therefore, the 1 cm sample from a deeper depth interval (between 5–8 cm depths) of the sediment was utilized. These sediments were retrieved from water depths ranging between ~600 and 2300 m (Trommer et al., 2009).

2.2. GDGT analysis

The lipid extraction methods used for the Mediterranean Sea and the Red Sea surface sediments were described previously in Kim et al. (2015) and Trommer et al. (2009), respectively. The original polar fractions of the extracts of the surface sediments were re-analyzed by dissolving it in hexane:isopropanol (99:1, v/v), filtered through a 0.45 μm PTFE filter, and analyzed with ultra-high performance liquid chromatography/ mass spectrometry (UHPLC/MS) on an Agilent 1260 Infinity HPLC coupled to an Agilent 6130 MSD according to Hopmans et al. (2016). The isoprenoid and branched GDGTs were detected by scanning for their $[M+H]^+$ ions (protonated mass), and OH-isoGDGTs were detected and quantified from the mass chromatograms of the $[M+H-18]^+$ ions (i.e., *m/z* 1300.3, 1298.3 and 1296.3) as suggested previously (Huguet et al., 2013). The OH-isoGDGTs were identified by comparing their retention times with an in-house standard sample derived from a sediment extract of Drammensfjord.

We calculated SST estimates from the indices, %OH (Equation (1); Huguet et al., 2013), RI-OH, RI-OH′ (Equations (3) and (5); Lü et al., 2015) and TEX_{86}^{OH} (Equation (7); Varma et al., 2024) according to 'NIOZ dataset' equations (Equations (2), (4), (6), (8)) from Varma et al. (2024).

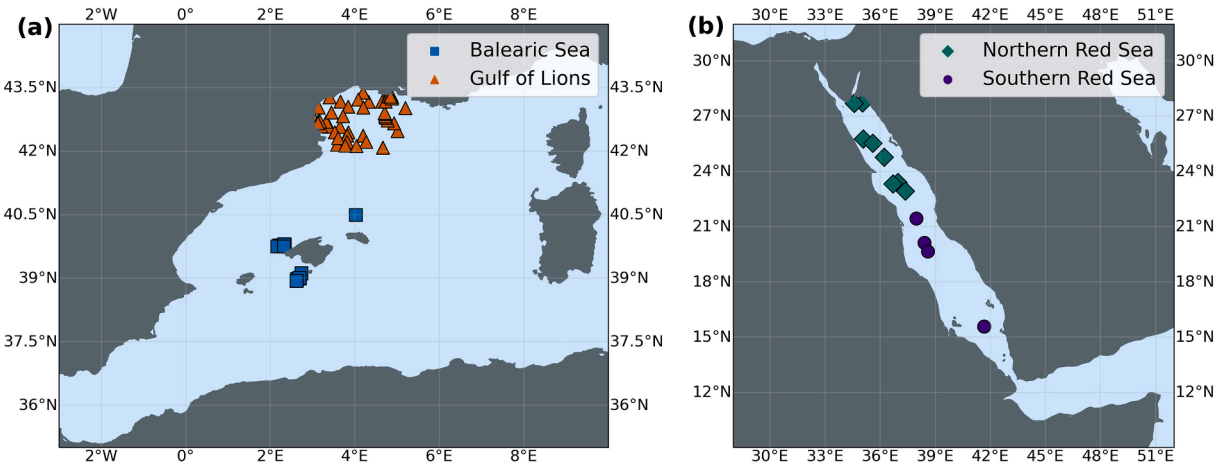

Fig. 1. Location of surface sediments used in this study from (a) Mediterranean Sea (b) Red Sea. Sediments from Gulf of Lions were previously published in Varma et al. (2024). (For interpretation of the references to colour in this figure legend, the reader is referred to the web version of this article.)

The global core-top calibration of Kim et al. (2010) (Equation (10)) was used to calculate TEX_{86}-based SSTs following Equation (9).

$$\%OH = \frac{[OH-0]+[OH-1]+[OH-2]}{[0]+[1]+[2]+[3]+[Cren]+[Cren']+[OH-0]+[OH-1]+[OH-2]} \times 100 \quad (1)$$

$$SST = \frac{\%OH - 6.79}{-0.227} \quad (2)$$

$$RI-OH = \frac{[OH-1]+2\times[OH-2]}{[OH-1]+[OH-2]} \quad (3)$$

$$SST = \frac{RI-OH-1.06}{0.021} \quad (4)$$

$$RI-OH' = \frac{[OH-1]+2\times[OH-2]}{[OH-0]+[OH-1]+[OH-2]} \quad (5)$$

$$SST = \frac{RI-OH'+0.11}{0.044} \quad (6)$$

$$TEX_{86}^{OH} = \frac{[2]+[3]+[Cren']}{[1]+[2]+[3]+[Cren']+[OH-0]} \quad (7)$$

$$SST = \frac{TEX_{86}^{OH}-0.033}{0.023} \quad (8)$$

$$TEX_{86}^{H} = \log\left(\frac{[2]+[3]+[Cren']}{[1]+[2]+[3]+[Cren']}\right) \quad (9)$$

$$SST = 68.4 \times TEX_{86}^{H} + 38.6 \quad (10)$$

[OH-n] indicates hydroxylated isoprenoidal GDGTs with n number of cyclopentane rings.

[n] indicates non-hydroxylated isoprenoidal GDGTs with n number of cyclopentane rings.

2.3. Statistical analysis

A Principal Component Analysis (PCA) was performed on the summed and standardized fractional abundances of regular isoGDGTs and OH-isoGDGTs along with environmental parameters from each location using the prcomp function in R software. Logarithmic correlations between various parameters utilized in this study were performed using statistical functions in python (scipy.stats).

3. Results

Seventy-six surface sediments from the Mediterranean Sea and fifteen surface sediments from the Red Sea were analyzed for regular isoGDGTs and OH-isoGDGTs. We first screened the data for sediments influenced by terrestrial input, as indicated by Branched and Isoprenoid Tetraether index (BIT) values (Hopmans et al., 2004; Weijers et al., 2006). Eight out of 57 sediments from the Gulf of Lions had BIT values >0.3 and were, therefore, removed from further consideration. The BIT index values for the Balearic and Red Sea sediments were all <0.1, suggesting that there is no major terrestrial influence on the isoGDGTs in these sediments.

The regular isoGDGTs distributions and the TEX_{86} values obtained by re-analysis of the sediment extracts using updated methodology are consistent with previously reported values for these sediments (Trommer et al., 2009; Kim et al., 2015). Indeed, this study confirms the previously observed large variations in the isoGDGT [2]/[3] ratios in the Balearic Sea and the Gulf of Lions, which ranged from ~3 to 7 and ~2 to 10, respectively (Kim et al., 2015). We also re-analyzed the Red Sea sediment samples and determined the isoGDGT [2]/[3] ratio for these sediments, which ranged from ~5 to 11 (See Supplementary data).

The abundance of OH-isoGDGTs in the sediments of the Balearic Sea varied from 1 to 3 % (Supplementary data), which is similar to the range observed in sediments from the Gulf of Lions, ranging from 1 to 4 % (Varma et al., 2024). In contrast, the %OH for the Red Sea sediments were all <1 % (Supplementary data). Note that only seven out of the fifteen surface sediments from the Red Sea contained detectable amounts of OH-isoGDGTs. These low abundances of OH-isoGDGTs are expected, since these sediments come from environments with relatively high temperatures (>19 °C and >25 °C, in the Mediterranean and the Red Sea, respectively), which generally contain low abundances of OH-isoGDGTs (Huguet et al., 2013; Varma et al., 2024). The OH-isoGDGTs mainly comprised OH-isoGDGT-0 and -1 in similar relative abundances (between 30 and 50 % of all OH-isoGDGTs), and lower abundances for OH-isoGDGT-2 (0–30 %) for the Mediterranean Sea sediments (Supplementary data). In contrast, for the Red Sea sediments, OH-isoGDGT-2 was the dominant OH-isoGDGT (40–60 % of all OH-isoGDGTs; Supplementary data) with lower abundances of OH-isoGDGT-0 and -1 (<30 %).

The values for RI-OH′ and RI-OH ranged from 0.59 to 1.01 and 1.25 to 1.49, respectively, for the Mediterranean Sea sediments, and 1.12–1.47 and 1.62–1.75, respectively, for the Red Sea sediments (Supplementary data). The TEX_{86} and TEX_{86}^{OH} proxy values ranged from

0.38 to 0.64 and 0.30–0.62, respectively, in the Mediterranean Sea and 0.77–0.88 and 0.76–0.88, respectively, in the Red Sea sediments. The low abundance of OH-isoGDGTs in the Red Sea sediments results in just minor differences between TEX_{86} and TEX_{86}^{OH} values.

4. Discussion

4.1. Factors controlling OH-isoGDGTs in the Mediterranean Sea and the Red Sea

To investigate the factors regulating OH-isoGDGT distributions in surface sediments from the Western Mediterranean Sea and the Red Sea, we performed a PCA on the summed and standardized fractional abundances of isoGDGTs and OH-isoGDGTs (Fig. 2). The principal components PC1 and PC2 explain 66.7 and 17.7 % of variance, respectively. The isoGDGT-0 and OH-isoGDGTs plot positively along PC1, while the remaining isoGDGTs, crenarchaeol, and its isomer plot negatively. When environmental factors were plotted alongside isoGDGT abundances and proxy indices, it becomes evident that isoGDGTs and the TEX_{86} are plotting along with water depth and not temperature (Fig. 2), consistent with Kim et al. (2015). In contrast, OH-isoGDGTs plot opposite to water depth and nearly orthogonally to SST. This suggests that abundance of OH-isoGDGTs is negatively impacted by water depth, with a minor influence from temperature. Indeed, for global marine surface sediments, it was also shown that water depth has an impact on OH-isoGDGT-1 and -2, but not on OH-isoGDGT-0, which was primarily controlled by temperature (Varma et al., 2024). Interestingly, although the abundance of OH-isoGDGTs seems mainly controlled by water depth in these basins, the degree of cyclization of OH-isoGDGTs, as reflected in the RI-OH and RI-OH′ proxy indices, were more strongly associated with SST and not water depth. OH-GDGT proxies, particularly RI-OH and RI-OH′, did not show any influence of salinity, although some correlations with salinity were observed for TEX_{86} and TEX_{86}^{OH} in the Mediterranean Sea (not shown here). Below we discuss these factors affecting the isoGDGT and OH-isoGDGT distributions, as well as the proxies derived from them.

4.2. Influence of water depth on OH-isoGDGTs

When we plot the fractional abundance of isoGDGTs with water depth, we observe similar trends as Kim et al. (2015) for isoGDGT-2 and crenarchaeol isomer, where they increase with water depth (Fig. 3). A similar pattern is observed for the Red Sea sediments. We also observe that the Balearic Sea and Gulf of Lions sediments form different clusters when isoGDGT-1 and -3 are plotted with water depth, in contrast to other isoGDGTs.

When the abundance of OH-isoGDGTs, as summed and standardized fractional abundances of all isoGDGTs and OH-isoGDGTs, is plotted with water depth, we observe a substantial decrease in relative abundance of OH-isoGDGTs for the Mediterranean Sea sediments, in particular at water depths shallower than 500 m (Fig. 3). Although limited data points exist for the Red Sea sediments, OH-isoGDGT-2, the most abundant OH-isoGDGT in the Red Sea, also shows a tendency to decrease with water depth (Fig. 3c).

The observed changes in distributions of isoGDGTs have been previously assigned to different thaumarchaeotal communities (Kim et al., 2015; Besseling et al., 2019). The isoGDGT [2]/[3] ratio serves as an indicator of different archaeal communities that inhabit the water column, with high values (>5) indicative of the contribution of deep-water archaeal communities (Taylor et al., 2013; Villanueva et al., 2015; Besseling et al., 2019). In our dataset, we observe correlations of fractional abundances of isoGDGT and OH-isoGDGT with the isoGDGT [2]/[3] ratio, i.e., isoGDGT-2 and cren' reveal strong positive correlations and OH-isoGDGTs show strong negative correlations with isoGDGT [2]/[3] ratio (Supplementary Fig. 1). This suggests that deep thaumarchaeotal communities might have a much lower abundance of OH-isoGDGTs in their lipid composition than shallow water communities. All Red Sea sediments have isoGDGT [2]/[3] ratio >5, as expected with

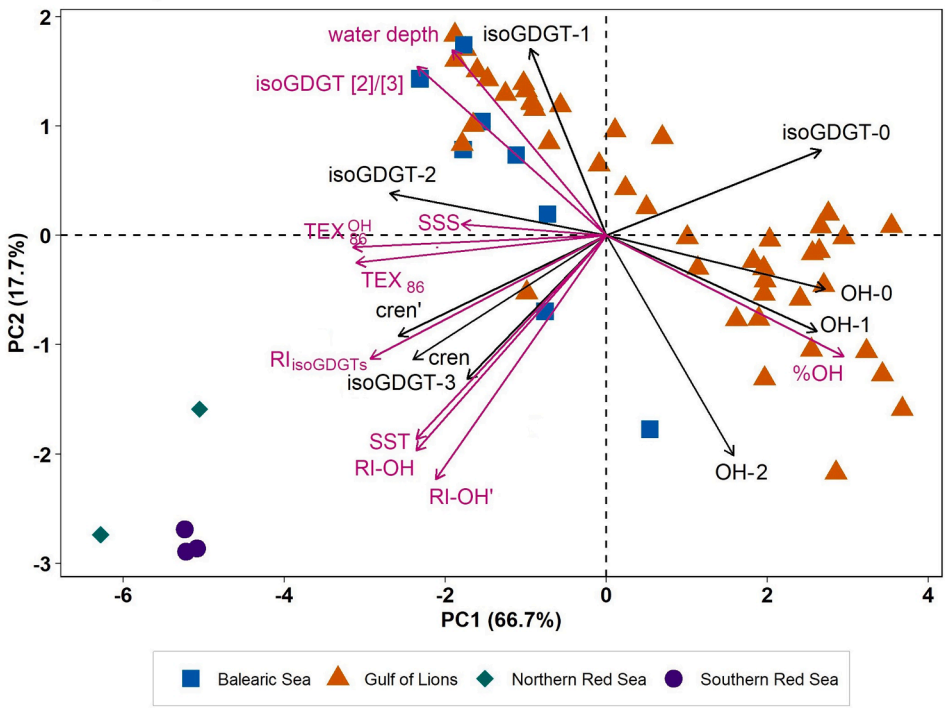

Fig. 2. Principal component analysis on the summed and standardized fractional abundances of hydroxylated and non-hydroxylated isoGDGTs and proxies based on them from the Mediterranean Sea and the Red Sea surface sediments. Loadings for the proxies derived from isoGDGTs and OH-isoGDGTs, and for environmental variables obtained from the location of the surface sediments using satellite temperature data or World Ocean Atlas (Locarnini et al., 2019; Zweng et al., 2019) are in pink. (For interpretation of the references to colour in this figure legend, the reader is referred to the web version of this article.)

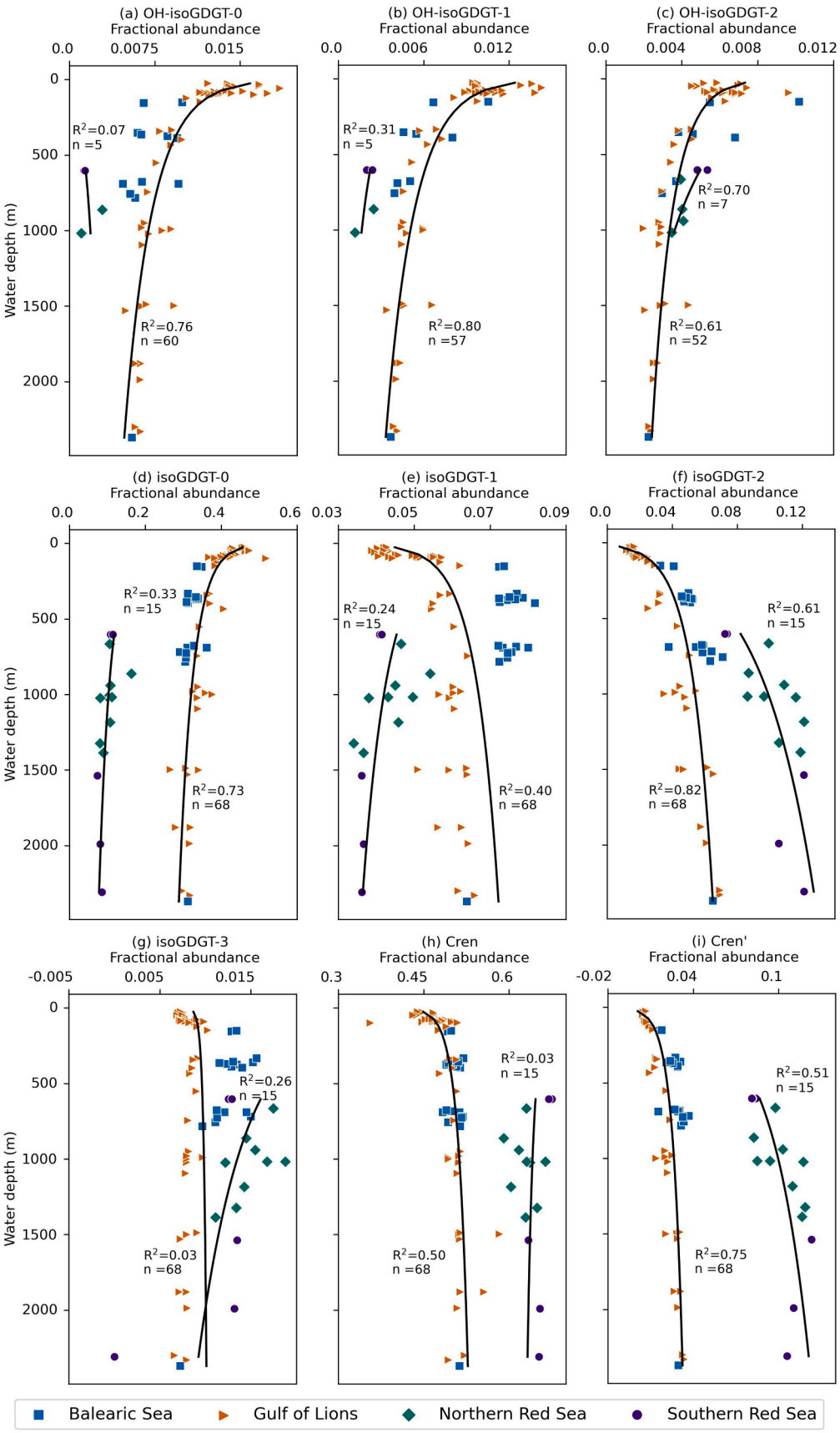

Fig. 3. Fractional abundance of individual isoGDGTs and OH-isoGDGTs relative to that of all OH-isoGDGTs and isoGDGTs versus water depth of the surface sediment from the Mediterranean Sea and the Red Sea. Logarithmic correlations for the Mediterranean Sea and the Red Sea are plotted with their correlation coefficient (R^2) values. (For interpretation of the references to colour in this figure legend, the reader is referred to the web version of this article.)

the water depths of these sediments which are >500 m for all the sediments. This likely explains why the decrease in the abundance of the OH-isoGDGTs with water depth is weaker in the Red Sea dataset than observed in the Mediterranean Sea where the strongest decrease occurs at <500 m.

4.3. Impact of water depth on OH-isoGDGT-based proxies

Consistent with Kim et al. (2015), a strong positive correlation between the TEX_{86} and water depth was observed for both the Mediterranean Sea (correlation $R^2 = 0.88$, $p < 0.05$) and also the Red Sea ($R^2 = 0.56$, $p < 0.05$) (Fig. 4). The lower correlation coefficient for the Red Sea can be attributed to the lack of surface sediment samples from shallower depths (i.e., from depths <500 m), where a more pronounced decrease in TEX_{86} values is observed in the Mediterranean Sea. Kim et al. (2015) proposed that higher contribution of isoGDGTs at deep sites (>1000 m) in the Mediterranean Sea compared to open ocean settings, possibly originating from deep thaumarchaeotal communities with a different isoGDGT composition (see Section 4.2), might result in high TEX_{86} values and a warm bias in temperature estimates using a global open ocean calibration. Conversely, TEX_{86} values derived from shallow Mediterranean sites (<1000 m water depth) have been shown to underestimate SSTs relative to satellite-derived temperatures (Kim et al., 2015).

The TEX_{86}^{OH} index, which incorporates OH-isoGDGT-0 in its denominator (Varma et al., 2024), also exhibited a strong correlation with water depth and the isoGDGT [2]/[3] ratio, due to two factors: 1) the negative correlation between OH-isoGDGT-0 and water depth and 2) the relatively low abundance of OH-isoGDGT-0 making the differences between TEX_{86} and TEX_{86}^{OH} relatively small (Fig. 4, Supplementary Fig. 2). This influence of water depth also becomes evident when we plot the TEX_{86}^{OH} data in the global surface sediment dataset (from Varma et al., 2024) plotted against SST (Fig. 5). While a general correlation between SST and TEX_{86}^{OH} (and TEX_{86}; Kim et al., 2015) is observed, the Mediterranean Sea sediments exhibit a large range of TEX_{86}^{OH} values for a small range of temperatures, with deep sites (>1000 m) having higher values

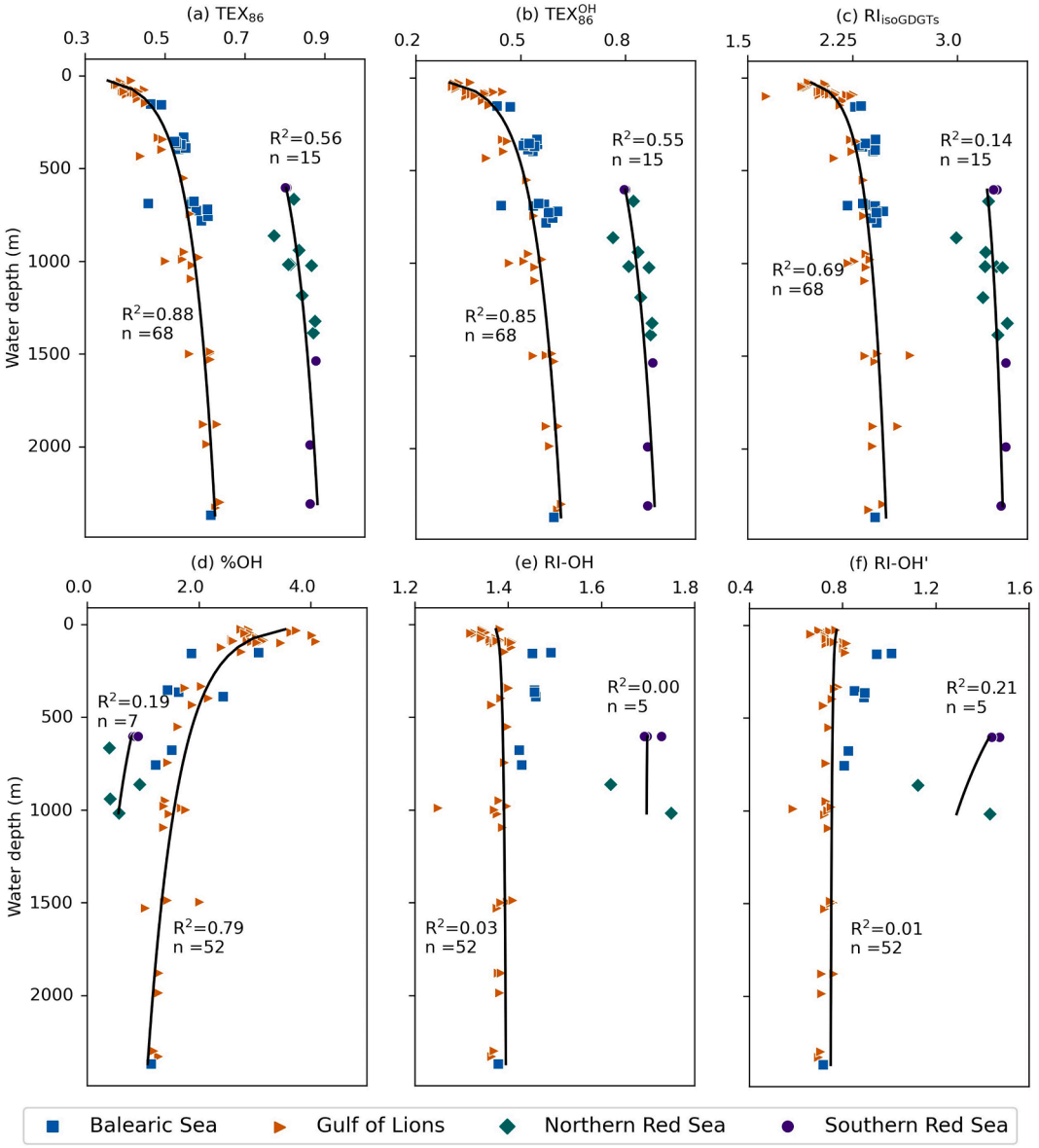

Fig. 4. Plots of isoGDGT- and OH-isoGDGT- based proxies with water depth for surface sediments from the Mediterranean Sea and the Red Sea. Logarithmic correlations for the Mediterranean Sea and the Red Sea are plotted with their correlation coefficient (R^2) values. (For interpretation of the references to colour in this figure legend, the reader is referred to the web version of this article.)

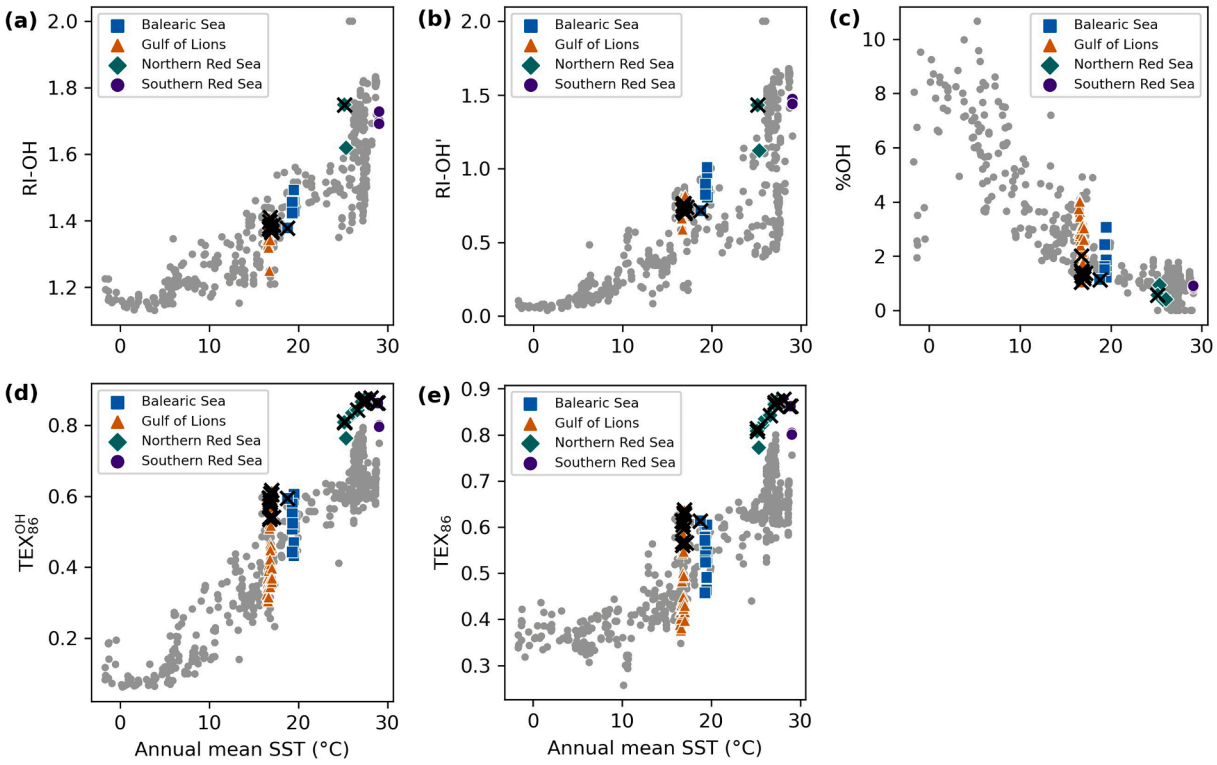

Fig. 5. Correlations of OH-isoGDGT- and isoGDGT-based proxies with annual mean sea surface temperature for surface sediments from the global ocean. Surface sediments from Varma et al. (2024) are shown here in grey. Crosses denote surface sediments from the Mediterranean Sea and the Red Sea from water depths >1000 m. (For interpretation of the references to colour in this figure legend, the reader is referred to the web version of this article.)

compared to the shallow sites. A separate 'Red Sea cluster' in the plot of TEX_{86} versus SST has been reported previously and a regional TEX_{86}-SST relationship was suggested (Trommer et al., 2009; Inglis et al., 2015). A similar separate 'Red Sea cluster' for the TEX_{86}^{OH} plotted against SST is also observed (Fig. 5) which is not surprising due to the extremely low abundance of OH-isoGDGTs in the Red Sea.

Consistent with the decrease in abundance of all the OH-isoGDGTs with increasing depth (see Section 4.2), the %OH also shows a strong decrease with water depth in the Mediterranean Sea sediments, in particular in the upper 1000 m (Fig. 4d). This is contrary to what we expect if OH-isoGDGT abundance is controlled solely by temperature, i.e., a higher %OH at deeper depths where the water temperature is lower. This is a similar trend as the TEX_{86} index which increases with depth (Fig. 4a) despite that deep-water temperatures are lower. This suggests that also for %OH, the contribution of deep-water thaumarchaeota leads to an overestimation of temperatures inferred from the %OH values. In the case of the Red Sea sediments, the OH-isoGDGT abundance is quite low and remains below the detection limit for sediments from depths deeper than ~1000 m (Fig. 4). However, the %OH values from the Red Sea do seem to match those of other tropical regions and do not form a separate cluster, likely due to their overall low abundances (Fig. 5).

Interestingly, when we plot the fractional abundance of OH-isoGDGTs normalized to all OH-isoGDGTs, rather than the sum of isoGDGTs and OH-isoGDGTs, we observe no significant decrease with water depth for all three OH-isoGDGTs (Supplementary Fig. 3). Indeed, RI-OH′ and RI-OH do not decrease significantly with water depth (Fig. 4e, 4f) in agreement with our PCA results (Fig. 2). For comparison, we plotted the Ring Index of regular isoGDGTs ($RI_{isoGDGTs}$; Zhang et al., 2016), the isoGDGT equivalent of the RI-OH′, with water depth in our dataset. We observe that unlike RI-OH′, the $RI_{isoGDGTs}$ significantly increases with water depth (Fig. 4c). This suggests that a different mechanism is responsible for the observed patterns in RI-OH′ and RI-OH compared to isoGDGTs, i.e., the degree of cyclization of OH-isoGDGTs may be similar for shallow and deep water thaumarchaeota in contrast to the degree of cyclization of isoGDGTs. Our observations are in strong contrast to those for other tropical regions where a strong water depth dependence was observed for RI-OH′ and RI-OH (Varma et al., 2024). Interestingly, unlike with the TEX_{86} and TEX_{86}^{OH}, there is no distinct 'Red Sea cluster' in the global dataset of RI-OH and RI-OH′ against SST (Fig. 5). However, this could also be due to the overall low abundance of OH-isoGDGTs and the larger spread of data in tropical regions for RI-OH and RI-OH′ due to the impact of water depth on these proxies (Xiao et al., 2023; Varma et al., 2024).

4.4. Implications

The results obtained for the OH-isoGDGT proxies demonstrate remarkable parallels with those obtained for the isoGDGT proxies, i.e., a strong impact of water depth is found for TEX_{86}, TEX_{86}^{OH} and %OH, in the Mediterranean Sea and the Red Sea, in contrast to open marine tropical environments. Conversely, water depth exhibits a pronounced impact on RI-OH and RI-OH′ in open marine tropical environments (Xiao et al., 2023; Varma et al., 2024), while this is not observed for the Mediterranean Sea. We speculate that such contrasting patterns observed for these proxies in the Mediterranean Sea compared to the open ocean settings might be due to different lipid distributions of the shallow and deep water archaeal communities, which somehow is more evident in saline semi-enclosed basins with relatively warm bottom water temperatures than in open oceans. Phylogenetic, ecological, or sedimentological (modes of transport) factors may underlie these patterns, but the exact mechanism remains to be elucidated.

While a definitive explanation for these observations remains elusive at present, we can infer some implications for the application of OH-isoGDGTs-based proxies in the Mediterranean Sea. Firstly, since the TEX_{86}^{OH} index also exhibits a similar strong impact of water depth as the TEX_{86}, the application of this proxy in this region will suffer from the

same biases as TEX_{86}. Kim et al. (2015) observed a distinct TEX_{86}^{H}-SST relationship for deep-water sediments (>1000 m) from the semi-enclosed basins of the Mediterranean Sea and the Red Sea, compared to the global dataset. Unfortunately, due to limited geographical coverage of the surface sediments employed in this study from the deep sites in the Mediterranean Sea, it is currently not possible to test the hypothesis that the TEX_{86}^{OH} from deep water sediments may exhibit a similar strong correlation with SST. With respect to %OH as a temperature proxy, its strong correlation with water depth (Fig. 5) will also prohibit a direct application of it as a temperature proxy. Further analysis with geographically more distributed sediments from the Mediterranean Sea needs to be done to examine if %OH will also exhibit a distinct correlation with SST for sediments from water depths >1000 m.

In contrast to these proxies, the RI-OH and RI-OH′ exhibit no significant correlation with water depth (Fig. 4) and have lowest residual errors in predicting temperature among the proxies analyzed for the sediments from the Mediterranean Sea (Supplementary Fig. 4). The RI-OH and RI-OH′ have previously been applied to reconstruct temperature changes over the last several glacial cycles, and shown promising results (Davtian et al., 2019; Morcillo-Montalbá et al., 2021). For example, Davtian et al. (2019) have shown that RI-OH provides better temperature estimates compared to TEX_{86} in a shallow sediment core from the western Mediterranean Sea. Our results support their assumption that RI-OH and RI-OH′ may serve as a more suitable temperature proxy than the TEX_{86} in the Mediterranean Sea. However, the potential influence of terrestrial input on ring indices of OH-isoGDGTs in the Mediterranean Sea warrants further investigation, as previously suggested by Kang et al. (2017) in the Han River system. Although RI-OH and RI-OH′ show large residuals in the Red Sea (Supplementary Fig. 4), they fall within the range of values observed for surface sediments in other tropical oceans (Fig. 5). Hence, unlike for regular isoGDGTs, the endemic archaeal communities of the Red Sea may not have a distinct OH-isoGDGT composition compared to open ocean in tropical regions. However, because there is a very low abundance of OH-isoGDGTs in the Red Sea, it is unlikely that the RI-OH and RI-OH′ are suitable as a temperature proxy in this region.

5. Conclusions

The OH-isoGDGTs in surface sediments of the Mediterranean Sea and the Red Sea reveals distinct patterns. The abundances of individual OH-isoGDGTs relative to the total isoGDGTs and OH-isoGDGTs decrease substantially with increasing water depth and isoGDGT [2]/[3] ratio in the Mediterranean Sea. This suggests that the relative abundance of OH-isoGDGTs varies among the different archaeal communities in the water column. Consequently, this affects OH-isoGDGT-based temperature proxies in the Mediterranean Sea, such as the abundance of OH-isoGDGTs (%OH), which shows a strong decreasing trend with water depth. Furthermore, the TEX_{86}^{OH} shows a strong increase with water depth, similar to TEX_{86}, due to the decreasing abundance of OH-isoGDGT-0 with water depth and the relatively lower abundances of OH-isoGDGTs compared to regular isoGDGTs. This leads to warm biases in the temperature reconstructed from %OH and TEX_{86}^{OH} at deep sites.

The ring indices of OH-isoGDGTs (RI-OH and RI-OH′), however, do not show a significant trend with water depth in the Mediterranean Sea and seem to be influenced more by temperature. Interestingly, this is in contrast to the observations for regular isoGDGTs, where the ring index ($RI_{isoGDGTs}$) and TEX_{86} values show correlations with water depth and much less with temperature. These findings highlight the potential of RI-OH and RI-OH′ as temperature proxies in the Mediterranean region.

Finally, the %OH, RI-OH and RI-OH′ indices did not exhibit a distinct 'Red Sea cluster' which is observed for TEX_{86} index in the global core-top dataset. Instead, these indices exhibited values similar to those observed in other tropical oceans. However, the extremely low abundance of OH-isoGDGTs (<1%) in the Red Sea, strongly limits the applicability of OH-isoGDGT-based temperature proxies in this region.

CRediT authorship contribution statement

Devika Varma: Writing – original draft, Visualization, Investigation, Formal analysis, Data curation, Conceptualization. **Marcel T.J. van der Meer:** Writing – review & editing. **Gert-Jan Reichart:** Writing – review & editing. **Stefan Schouten:** Writing – review & editing, Visualization, Funding acquisition, Conceptualization.

Declaration of competing interest

The authors declare that they have no known competing financial interests or personal relationships that could have appeared to influence the work reported in this paper.

Data availability

All data related to this article is available online through: https://dataportal.nioz.nl/doi/10.25850/nioz/7b.b.8g. The data is also uploaded in Supplementary materials as Supplementary data.

Acknowledgements

We thank Monique Verweij and Denise Dorhout for analytical support. Michal Kucera is thanked for providing sediments from the Red Sea. We thank Dr. Nina Davtian and an anonymous reviewer for their comments which improved the manuscript. This work was carried out under the program of the Netherlands Earth System Science Centre (NESSC), financially supported by the Ministry of Education, Culture and Science (OCW) through grant 024.002.001 to SS. This project has received funding from the European Union's Horizon 2020 research and innovation programme under the Marie Skłodowska-Curie, grant agreement No. 847504.

Appendix A. Supplementary material

Supplementary data to this article can be found online at https://doi.org/10.1016/j.orggeochem.2024.104780.

References

Basse, A., Zhu, C., Versteegh, G.J.M., Fischer, G., Hinrichs, K.U., Mollenhauer, G., 2014. Distribution of intact and core tetraether lipids in water column profiles of suspended particulate matter off Cape Blanc, NW Africa. Organic Geochemistry 72, 1–13.

Besseling, M.A., Hopmans, E.C., Koenen, M., van der Meer, M.T.J., Vreugdenhil, S., Schouten, S., Sinninghe Damsté, J.S., Villanueva, L., 2019. Depth-related differences in archaeal populations impact the isoprenoid tetraether lipid composition of the Mediterranean Sea water column. Organic Geochemistry 135, 16–31.

Davtian, N., Ménot, G., Fagault, Y., Bard, E., 2019. Western Mediterranean Sea paleothermometry over the Last Glacial Cycle based on the novel RI-OH index. Paleoceanography and Paleoclimatology 34, 616–634.

Eder, W., Schmidt, M., Koch, M., Garbe-Schönberg, D., Huber, R., 2002. Prokaryotic phylogenetic diversity and corresponding geochemical data of the brine–seawater interface of the Shaban Deep, Red Sea. Environmental Microbiology 4, 758–763.

Elling, F.J., Könneke, M., Nicol, G.W., Stieglmeier, M., Bayer, B., Spieck, E., de la Torre, J.R., Becker, K.W., Thomm, M., Prosser, J.I., Herndl, G.J., Schleper, C., Hinrichs, K.U., 2017. Chemotaxonomic characterisation of the thaumarchaeal lipidome. Environmental Microbiology 19, 2681–2700.

Grauel, A.L., Leider, A., Goudeau, M.L.S., Müller, I.A., Bernasconi, S.M., Hinrichs, K.U., de Lange, G.J., Zonneveld, K.A.F., Versteegh, G.J.M., 2013. What do SST proxies really tell us? A high-resolution multiproxy ($U^{K'}_{37}$, TEX^{H}_{86} and foraminifera $\delta^{18}O$) study in the Gulf of Taranto, central Mediterranean Sea. Quaternary Science Reviews 73, 115–131.

Hernández-Sánchez, M.T., Woodward, E.M.S., Taylor, K.W.R., Henderson, G.M., Pancost, R.D., 2014. Variations in GDGT distributions through the water column in the South East Atlantic Ocean. Geochimica et Cosmochimica Acta 132, 337–348.

Hopmans, E.C., Weijers, J.W.H., Schefuß, E., Herfort, L., Sinninghe Damsté, J.S., Schouten, S., 2004. A novel proxy for terrestrial organic matter in sediments based on branched and isoprenoid tetraether lipids. Earth and Planetary Science Letters 224, 107–116.

Hopmans, E.C., Schouten, S., Sinninghe Damsté, J.S., 2016. The effect of improved chromatography on GDGT-based palaeoproxies. Organic Geochemistry 93, 1–6.
Huguet, C., Schimmelmann, A., Thunell, R., Lourens, L.J., Sinninghe Damsté, J.S., Schouten, S., 2007. A study of the TEX_{86} paleothermometer in the water column and sediments of the Santa Barbara Basin, California. Paleoceanography 22, PA3203.
Huguet, C., Martrat, B., Grimalt, J.O., Sinninghe Damsté, J.S., Schouten, S., 2011. Coherent millennial-scale patterns in $U^{K'}_{37}$ and TEX^{H}_{86} temperature records during the penultimate interglacial-to-glacial cycle in the western Mediterranean. Paleoceanography 26, PA2218.
Huguet, C., Fietz, S., Rosell-Melé, A., 2013. Global distribution patterns of hydroxy glycerol dialkyl glycerol tetraethers. Organic Geochemistry 57, 107–118.
Huguet, C., Fietz, S., Rosell-Melé, A., Daura, X., Costenaro, L., 2017. Molecular dynamics simulation study of the effect of glycerol dialkyl glycerol tetraether hydroxylation on membrane thermostability. Biochimica et Biophysica Acta - Biomembranes 1859, 966–974.
Hurley, S.J., Lipp, J.S., Close, H.G., Hinrichs, K.U., Pearson, A., 2018. Distribution and export of isoprenoid tetraether lipids in suspended particulate matter from the water column of the Western Atlantic Ocean. Organic Geochemistry 116, 90–102.
Inglis, G.N., Farnsworth, A., Lunt, D., Foster, G.L., Hollis, C.J., Pagani, M., Jardine, P.E., Pearson, P.N., Markwick, P., Galsworthy, A.M.J., Raynham, L., Taylor, K.W.R., Pancost, R.D., 2015. Descent toward the Icehouse: Eocene sea surface cooling inferred from GDGT distributions. Paleoceanography 30, 1000–1020.
Jia, G., Zhang, J., Chen, J., Peng, P., Zhang, C.L., 2012. Archaeal tetraether lipids record subsurface water temperature in the South China Sea. Organic Geochemistry 50, 68–77.
Jia, G., Wang, X., Guo, W., Dong, L., 2017. Seasonal distribution of archaeal lipids in surface water and its constraint on their sources and the TEX_{86} temperature proxy in sediments of the South China Sea. Journal of Geophysical Research: Biogeosciences 122, 592–606.
Kang, S., Shin, K.H., Kim, J.H., 2017. Occurrence and distribution of hydroxylated isoprenoid glycerol dialkyl glycerol tetraethers (OH-GDGTs) in the Han River system, South Korea. Acta Geochimica 36, 367–369.
Kim, J.H., van der Meer, J., Schouten, S., Helmke, P., Willmott, V., Sangiorgi, F., Koç, N., Hopmans, E.C., Sinninghe Damsté, J.S., 2010. New indices and calibrations derived from the distribution of crenarchaeal isoprenoid tetraether lipids: Implications for past sea surface temperature reconstructions. Geochimica et Cosmochimica Acta 74, 4639–4654.
Kim, J.H., Schouten, S., Rodrigo-Gámiz, M., Rampen, S., Marino, G., Huguet, C., Helmke, P., Buscail, R., Hopmans, E.C., Pross, J., Sangiorgi, F., Middelburg, J.B.M., Sinninghe Damsté, J.S., 2015. Influence of deep-water derived isoprenoid tetraether lipids on the TEX^{H}_{86} paleothermometer in the Mediterranean Sea. Geochimica et Cosmochimica Acta 150, 125–141.
Kim, J.H., Villanueva, L., Zell, C., Sinninghe Damsté, J.S., 2016. Biological source and provenance of deep-water derived isoprenoid tetraether lipids along the Portuguese continental margin. Geochimica et Cosmochimica Acta 172, 177–204.
Leider, A., Hinrichs, K.U., Mollenhauer, G., Versteegh, G.J.M., 2010. Core-top calibration of the lipid-based $U^{K'}_{37}$ and TEX_{86} temperature proxies on the southern Italian shelf (SW Adriatic Sea, Gulf of Taranto). Earth and Planetary Science Letters 300, 112–124.
Liu, X.-L., Lipp, J.S., Simpson, J.H., Lin, Y.S., Summons, R.E., Hinrichs, K.U., 2012. Mono- and dihydroxyl glycerol dibiphytanyl glycerol tetraethers in marine sediments: Identification of both core and intact polar lipid forms. Geochimica et Cosmochimica Acta 89, 102–115.
Locarnini, R.A., Mishonov, A. V., Baranova, O.K., Boyer, T.P., Zweng, M.M., Garcia, H.E., Reagan, J.R., Seidov, D., Weathers, K.W., Paver, C.R., Smolyar, I. V., 2019. World Ocean Atlas 2018, Volume 1: Temperature. In: Mishonov, A., (Ed.). NOAA Atlas NESDIS 81, 52 pp.
Lü, X., Liu, X.L., Elling, F.J., Yang, H., Xie, S., Song, J., Li, X., Yuan, H., Li, N., Hinrichs, K. U., 2015. Hydroxylated isoprenoid GDGTs in Chinese coastal seas and their potential as a paleotemperature proxy for mid-to-low latitude marginal seas. Organic Geochemistry 89–90, 31–43.
MEDOC Group, 1970. Observation of formation of deep water in the Mediterranean Sea, 1969. Nature 227, 1037–1040.
Morcillo-Montalbá, L., Rodrigo-Gámiz, M., Martínez-Ruiz, F., Ortega-Huertas, M., Schouten, S., Sinninghe Damsté, J.S., 2021. Rapid climate changes in the Westernmost Mediterranean (Alboran Sea) over the last 35 kyr: New insights from four lipid paleothermometers ($U^{K'}_{37}$, TEX^{H}_{86}, RI-OH′, and LDI). Paleoceanography and Paleoclimatology 36, e2020PA004171. https://doi.org/10.1029/2020PA004171.
Nieto-Moreno, V., Martínez-Ruiz, F., Willmott, V., García-Orellana, J., Masqué, P., Sinninghe Damsté, J.S., 2013. Climate conditions in the westernmost Mediterranean over the last two millennia: an integrated biomarker approach. Organic Geochemistry 55, 1–10.
Polik, C.A., Elling, F.J., Pearson, A., 2018. Impacts of paleoecology on the TEX_{86} sea surface temperature proxy in the Pliocene-Pleistocene Mediterranean Sea. Paleoceanography and Paleoclimatology 33, 1472–1489.
Qian, P.Y., Wang, Y., Lee, O.O., Lau, S.C.K., Yang, J., Lafi, F.F., Al-Suwailem, A., Wong, T.Y.H., 2011. Vertical stratification of microbial communities in the Red Sea revealed by 16S rDNA pyrosequencing. The ISME Journal 5, 507–518.
Rattanasriampaipong, R., Zhang, Y.G., Pearson, A., Hedlund, B.P., Zhang, S., 2022. Archaeal lipids trace ecology and evolution of marine ammonia-oxidizing archaea. Proceedings of the National Academy of Sciences of the United States of America 119, e2123193119.
Rinke, C., Chuvochina, M., Mussig, A.J., Chaumeil, P.A., Davín, A.A., Waite, D.W., Whitman, W.B., Parks, D.H., Hugenholtz, P., 2021. A standardized archaeal taxonomy for the Genome Taxonomy Database. Nature Microbiology 6, 946–959.
Rohling, E., Abu-Zied, R., Casford, J.S.L., Hayes, A., Hoogakker, B.A., 2009. The marine environment: Present and past. In: Woodward, J. (Ed.), The Physical Geography of the Mediterranean. Oxford University Press, pp. 33–67.
Schouten, S., Hopmans, E.C., Schefuß, E., Sinninghe Damsté, J.S., 2002. Distributional variations in marine crenarchaeotal membrane lipids: a new tool for reconstructing ancient sea water temperatures? Earth and Planetary Science Letters 204, 265–274.
Schouten, S., Hopmans, E.C., Sinninghe Damsté, J.S., 2013. The organic geochemistry of glycerol dialkyl glycerol tetraether lipids: a review. Organic Geochemistry 54, 19–61.
Sinninghe Damsté, J.S., Schouten, S., Hopmans, E.C., Van Duin, A.C.T., Geenevasen, J.A. J., 2002. Crenarchaeol: The characteristic core glycerol dibiphytanyl glycerol tetraether membrane lipid of cosmopolitan pelagic crenarchaeota. Journal of Lipid Research 43, 1641–1651.
Sinninghe Damsté, J.S., Rijpstra, W.I.C., Hopmans, E.C., Jung, M.Y., Kim, J.G., Rhee, S. K., Stieglmeier, M., Schleper, C., 2012. Intact polar and core glycerol dibiphytanyl glycerol tetraether lipids of group I.1a and I.1b Thaumarchaeota in soil. Applied and Environmental Microbiology 78, 6866–6874.
Taylor, K.W.R., Huber, M., Hollis, C.J., Hernandez-Sanchez, M.T., Pancost, R.D., 2013. Re-evaluating modern and Palaeogene GDGT distributions: Implications for SST reconstructions. Global and Planetary Change 108, 158–174.
Tierney, J.E., 2014. Biomarker-based inferences of past climate: the TEX_{86} paleotemperature proxy. In: Treatise on Geochemistry, 2nd ed. Elsevier Ltd.
Trommer, G., Siccha, M., van der Meer, M.T.J., Schouten, S., Sinninghe Damsté, J.S., Schulz, H., Hemleben, C., Kucera, M., 2009. Distribution of Crenarchaeota tetraether membrane lipids in surface sediments from the Red Sea. Organic Geochemistry 40, 724–731.
Varma, D., Hopmans, E.C., van Kemenade, Z.R., Kusch, S., Berg, S., Bale, N.J., Sangiorgi, F., Reichart, G.J., Sinninghe Damsté, J.S., Schouten, S., 2024. Evaluating isoprenoidal hydroxylated GDGT-based temperature proxies in surface sediments from the global ocean. Geochimica et Cosmochimica Acta 370, 113–127.
Villanueva, L., Schouten, S., Sinninghe Damsté, J.S., 2015. Depth-related distribution of a key gene of the tetraether lipid biosynthetic pathway in marine Thaumarchaeota. Environmental Microbiology 17, 3527–3539.
Weijers, J.W.H., Schouten, S., Spaargaren, O.C., Sinninghe Damsté, J.S., 2006. Occurrence and distribution of tetraether membrane lipids in soils: implications for the use of the TEX_{86} proxy and the BIT index. Organic Geochemistry 37, 1680–1693.
Weijers, J.W.H., Lim, K.L.H., Aquilina, A., Sinninghe Damsté, J.S., Pancost, R.D., 2011. Biogeochemical controls on glycerol dialkyl glycerol tetraether lipid distributions in sediments characterized by diffusive methane flux. Geochemistry, Geophysics, Geosystems 12, Q100101-15.
Xiao, W., Xu, Y., Zhang, C., Lin, J., Wu, W., Xiaoxia, L., Tan, J., Zhang, X., Zheng, F., Song, X., Zhu, Y., Yang, Y., Zhang, H., Wenzhöfer, F., Rowden, A.A., Glud, R.N., 2023. Disentangling effects of sea surface temperature and water depth on hydroxylated isoprenoid GDGTs: insights from the hadal zone and global sediments. Geophysical Research Letters 50, e2023GL103109.
Zeng, Z., Liu, X.-L., Farley, K.R., Wei, J.H., Metcalf, W.W., Summons, R.E., Welander, P. V., 2019. GDGT cyclization proteins identify the dominant archaeal sources of tetraether lipids in the ocean. Proceedings of the National Academy of Sciences of the United States of America 116, 22505–22511.
Zhang, Y.G., Pagani, M., Wang, Z., 2016. Ring Index: a new strategy to evaluate the integrity of TEX_{86} paleothermometry. Paleoceanography 31, 220–232.
Zweng, M.M., Reagan, J.R., Seidov, D., Boyer, T.P., Antonov, J.I., Locarnini, R.A., Garcia, H.E., Mishonov, A. V., Baranova, O.K., Weathers, K.W., Paver, C.R., Smolyar, I. V., 2019. World Ocean Atlas 2018, Volume 2: Salinity. In: Mishonov, A., (ED.), NOAA Atlas NESDIS 82, 50p.